Electronic Supplementary Information

Cation Exchange-Induced Nickel Active Sites on FeOOH Cocatalyst for Enhanced Photoelectrochemical Water Oxidation of $BiVO_4$ Photoanode

*Mengxue Wang [a], Houjiang Liu [a], Yang Zhang [a], YuYao Zhang [a], Guijun Yang [a], Jiawei Ding [a], Yuanyuan Fu [a], Jin Cui [a], Zizhuang Li [a], Kai Song [a], Naiqin Zhao [a], Chunnian He [ab], Biao Chen [ab], Fang He [*a]*

[a] School of Materials Science and Engineering, Tianjin Key Laboratory of Composite and Functional Materials, Key Laboratory of Advanced Ceramics and Machining Technology (Ministry of Education), Tianjin University, Tianjin, P. R. China.

[b] National Industry-Education Platform of Energy Storage, Tianjin University, Tianjin, P. R. China

E-mail: fanghe@tju.edu.cn (F. He)

Supplementary Experimental Information

PEC Performance Measurements

PEC measurements were conducted at room temperature using a three-electrode testing system equipped with an electrochemical workstation (CHI660E). In this system, all samples served as the WE with a fixed exposed active area of 1 cm^2, while Pt and Ag/AgCl electrodes were employed as the CE and RE. The illumination source was a simulated sunlight AM 1.5G (100 $mW \cdot cm^{-2}$), and a 0.2 M Potassium borate (KBi) solution (pH =8.4) was used as the electrolyte. Current-voltage (J-V) curves were recorded at a scanning rate of 20 $mV \cdot s^{-1}$. The formula for potential conversion is as follows[1]:

$$E_{RHE} = E_{Ag/AgCl} + 0.197 + 0.059 \times pH \quad (1)$$

Where E_{RHE} refers to the converted potential versus RHE. The value of $E_{Ag/AgCl}$ is 0.1976 V at ambient temperature (25°C) and $E_{Ag/AgCl}$ is the obtained potential versus Ag/AgCl. Applied bias photon-to-current efficiency (ABPE) is calculated using the following equation[2]:

$$ABPE = \frac{I(mA \cdot cm^{-2}) \times (1.23 - V_{bias})(V)}{P_{lignt}(mW \cdot cm^{-2})} \quad (2)$$

Where I is the photocurrent density, V_{bias} is the applied potential, P_{light} is the incident illumination power density (100 mW·cm2). The incident photon-to-current conversion efficiency (IPCE) can be calculated by the following formula[3]:

$$IPCE = \frac{J_{ph}(mA \cdot cm^{-2}) \times 1240(V \times nm)}{\lambda(nm) \times P_{light}(mW \cdot cm^{-2})} \times 100\% \quad (3)$$

Where J_{ph} is the measured photocurrent density at specific wavelength, λ is the wavelength of incident light, and P_{light} is the measured light power intensity at that wavelength. The absorbed photon-to-current efficiency (APCE) can be calculated by the following formula[4].

$$APCE = \frac{IPCE}{LHE} \quad (4)$$

Where LHE is the light harvesting efficiency calculated using $LHE = 1 - 10^{-A(\lambda)}$, where A(λ) is the absorbance. The electrochemical impedance spectroscopy (EIS) was measured using small-amplitude alternating current signals ranging from 10^{-2} to 10^{5} Hz under 0.8 V_{RHE}. The charge injection efficiency (η_{inj}) and the charge separation efficiency (η_{sep})was calculated as the following equation[5]:

$$\eta_{inj} = J_{water}/J_{sulfite} \quad (5)$$

$$\eta_{sep} = J_{sulfite}/J_{abs} \quad (6)$$

Where $J_{sulfite}$ is the photocurrent density measured in 0.2 M potassium borate buffer with 0.2 M Na_2SO_3 electrolyte (pH=9.5), which serves as a hole scavenger and ensures the hole injection rate approaches 100%, and J_{water} is the photocurrent density measured in 0.2 M potassium borate buffer (pH=8.4). The J_{abs} is the photon adsorption rate expressed as the photocurrent density. The Faradaic efficiency can be determined as following equation[6].

$$\eta_{H_2} = \frac{2Fn_{H_2}}{Q} \quad (7)$$

Where F is Faraday constant (96485 $C \cdot mol^{-1}$), n is the production of hydrogen (mol), and Q is the amounts of charges generated by photocarriers (C). The charge carrier density (N_d) was calculated as following equation.

$$N_d = \frac{2}{e\varepsilon\epsilon_0}\left[\frac{d\frac{1}{C^2}}{dV}\right]^{-1} \quad (6)$$

The quantization using parameter D was calculated as following equation[7]:

$$D = I_t - I_s / I_m - I_s \quad (7)$$

where I_t, I_s and I_m are the time-dependent photocurrent, the steady-state photocurrent and the transient photocurrent spike, respectively. The electron lifetime (τ_r) is defined as the time at which lnD = -1.

DFT Computation

The OER reaction is a four-electron transfer process involving the modeling of intermediates *OH, *O, and *OOH:

$$* + OH^- \rightarrow * OH + e^-, \ \Delta G_1 \quad (8)$$

$$* OH + OH^- \rightarrow * O + e^- + H_2O, \ \Delta G_2 \quad (9)$$

$$* O + OH^- \rightarrow * OOH + e^-, \ \Delta G_3 \quad (10)$$

$$* OOH + OH^- \rightarrow O_2 + e^- + H_2O, \ \Delta G_2 \quad (11)$$

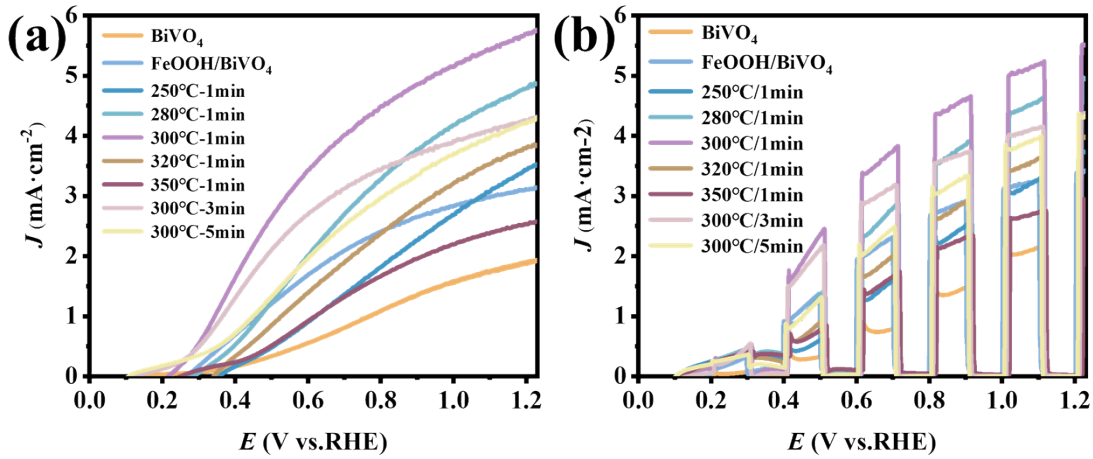

Figure S1. (a) Linear sweep voltammogram curves and (b) The transient photocurrent density curves of $BiVO_4$, $FeOOH/BiVO_4$ and $Ni:FeOOH/BiVO_4$ prepared at different temperatures and times.

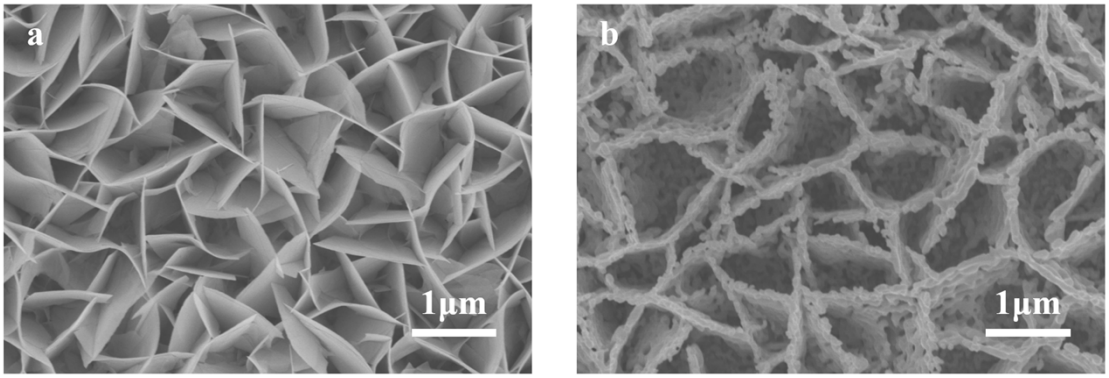

Figure S2. SEM images of (a) BiOI (b) $BiVO_4$ photoanodes.

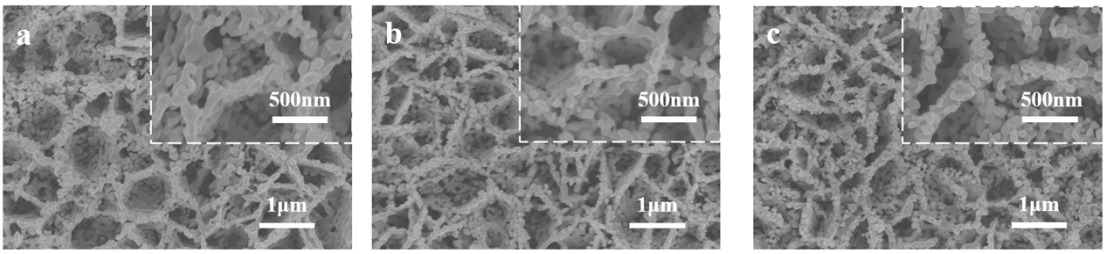

Figure S3. SEM images of (a) $BiVO_4$ (b) FeOOH/$BiVO_4$ and (c) Ni:FeOOH/$BiVO_4$.

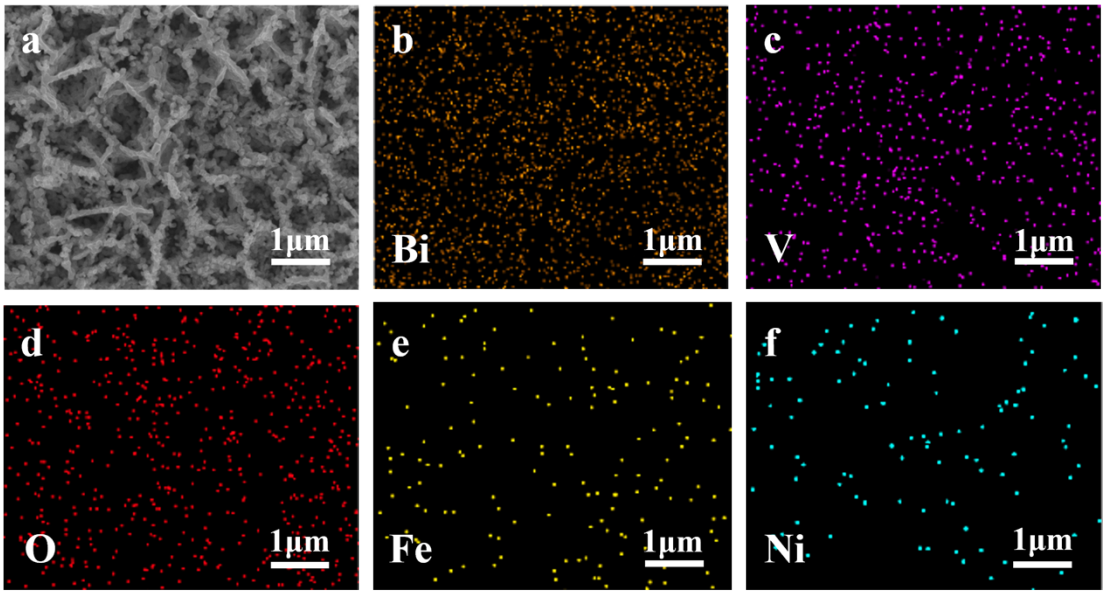

Figure S4. SEM EDS of Ni:FeOOH/$BiVO_4$.

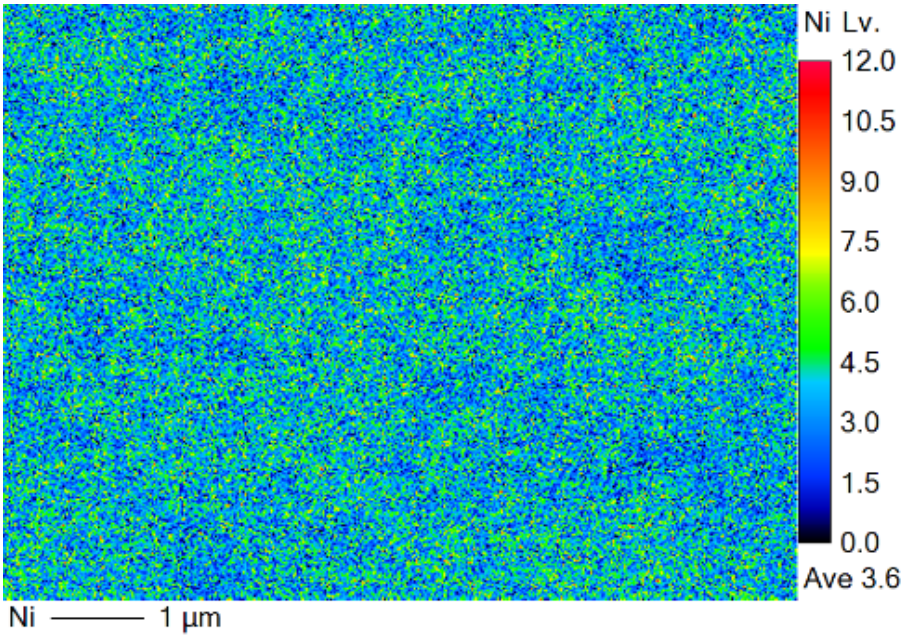

Figure S5. EPMA elemental mapping of Ni in Ni:FeOOH/$BiVO_4$.

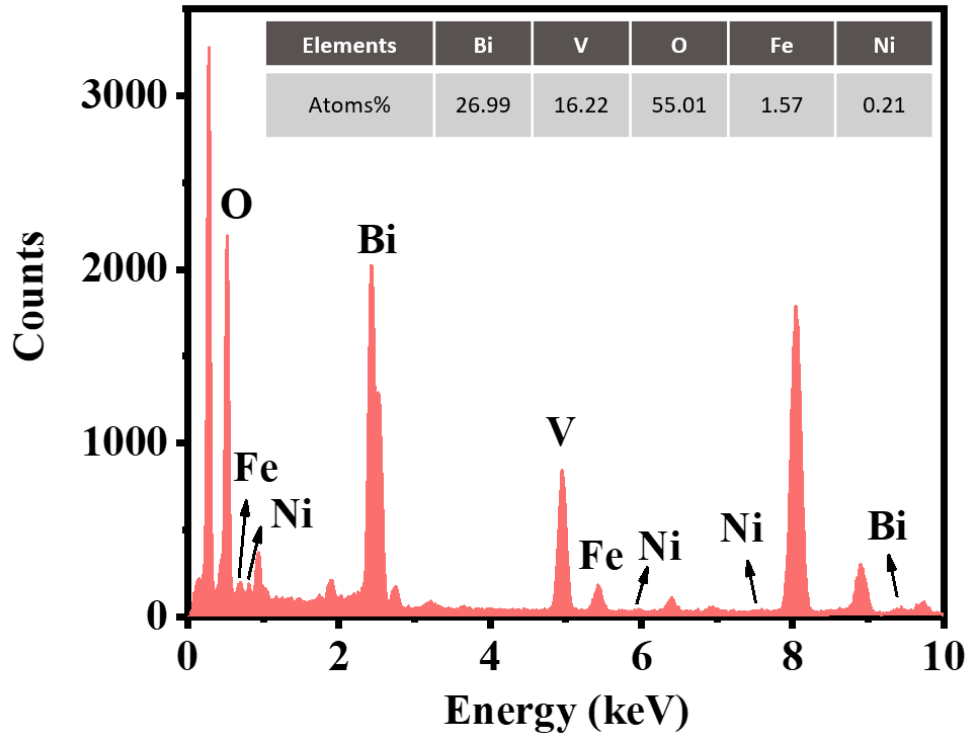

Figure S6. TEM EDS spectrum of Ni:FeOOH/$BiVO_4$.

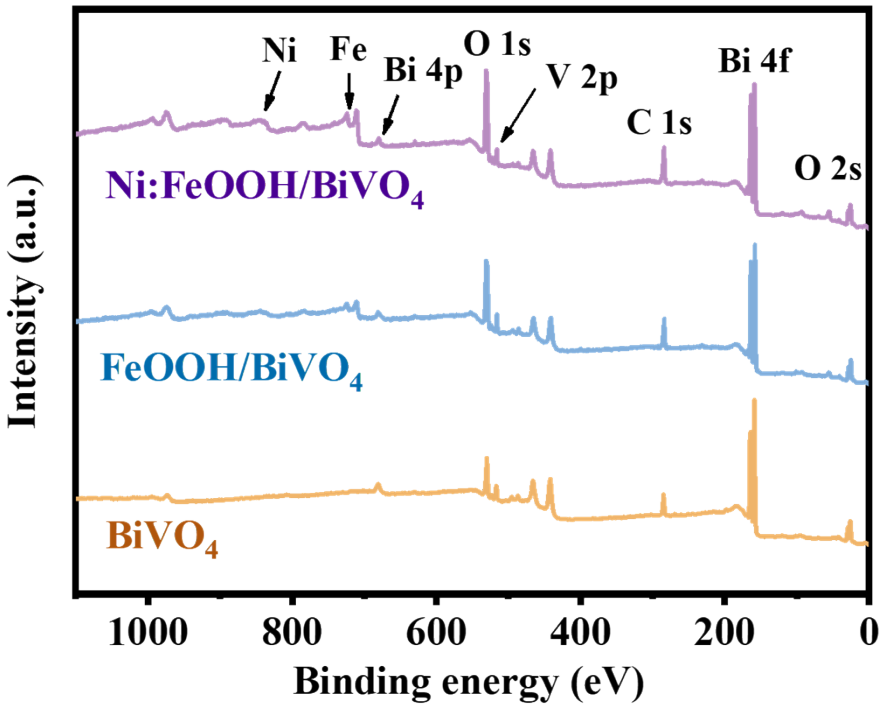

Figure S7. XPS survey spectra of $BiVO_4$, $FeOOH/BiVO_4$ and $Ni:FeOOH/BiVO_4$.

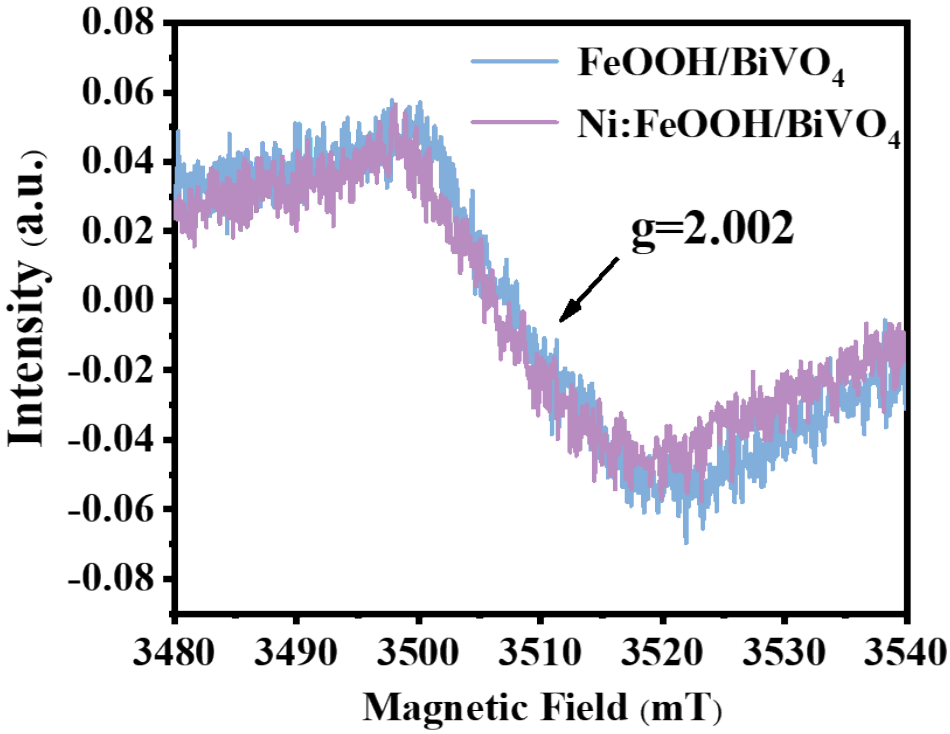

Figure S8. EPR spectra $FeOOH/BiVO_4$ and $Ni:FeOOH/BiVO_4$.

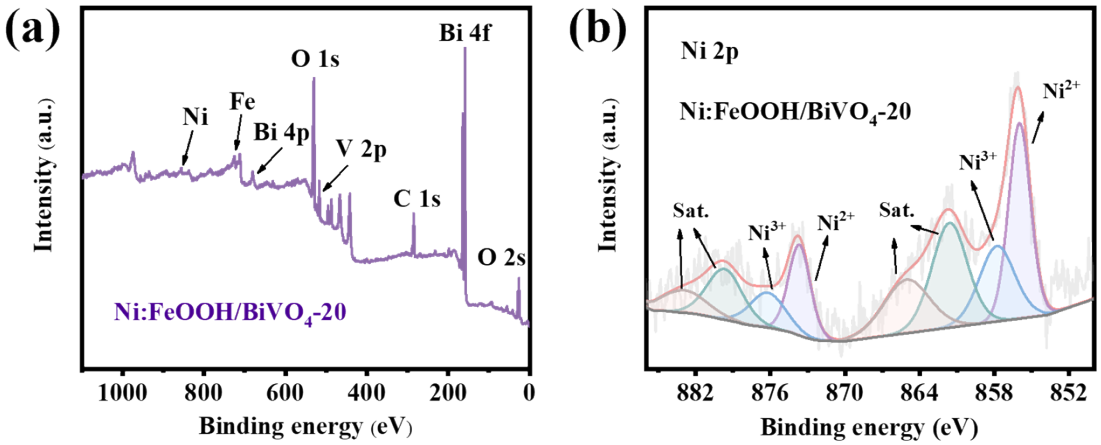

Figure S9. (a) XPS survey spectra (b) Ni 2p of Ni:FeOOH/$BiVO_4$ with replacement conditions of 300℃ for 20 minutes.

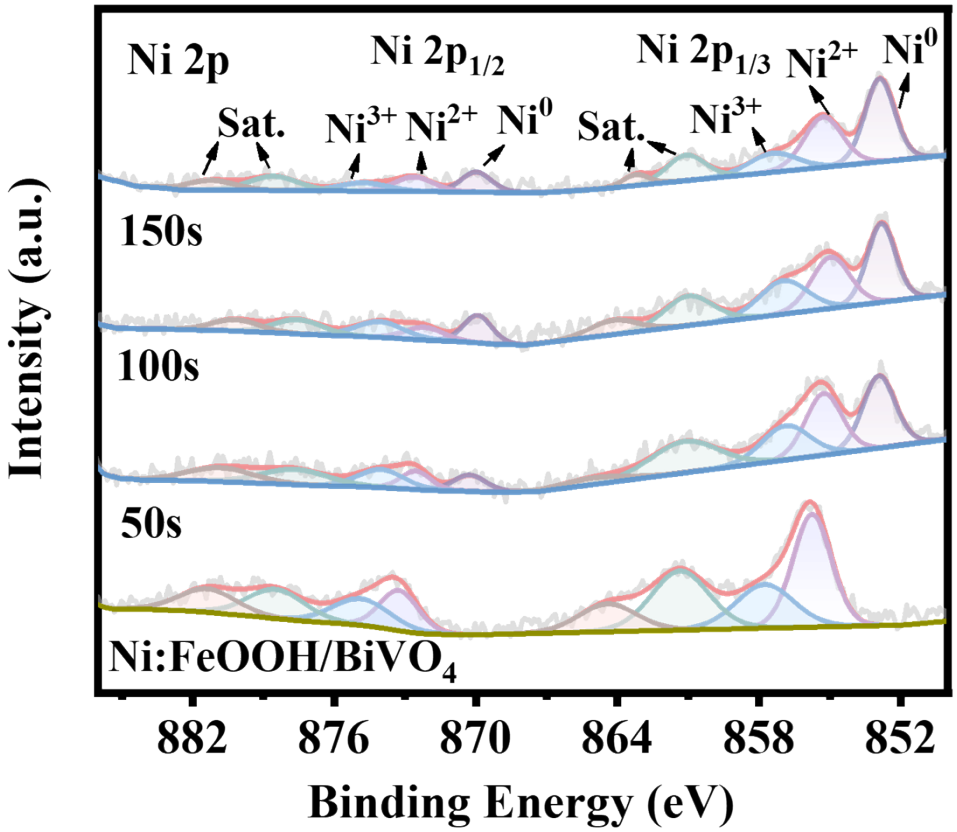

Figure S10. XPS survey spectra of Ni 2p in Ni:FeOOH/$BiVO_4$ with Ar^+ etching.

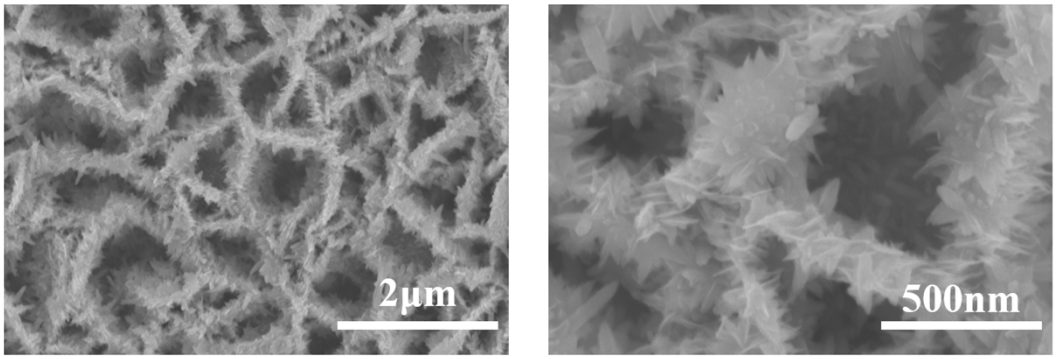

Figure S11. SEM EDS of α-FeOOH/$BiVO_4$.

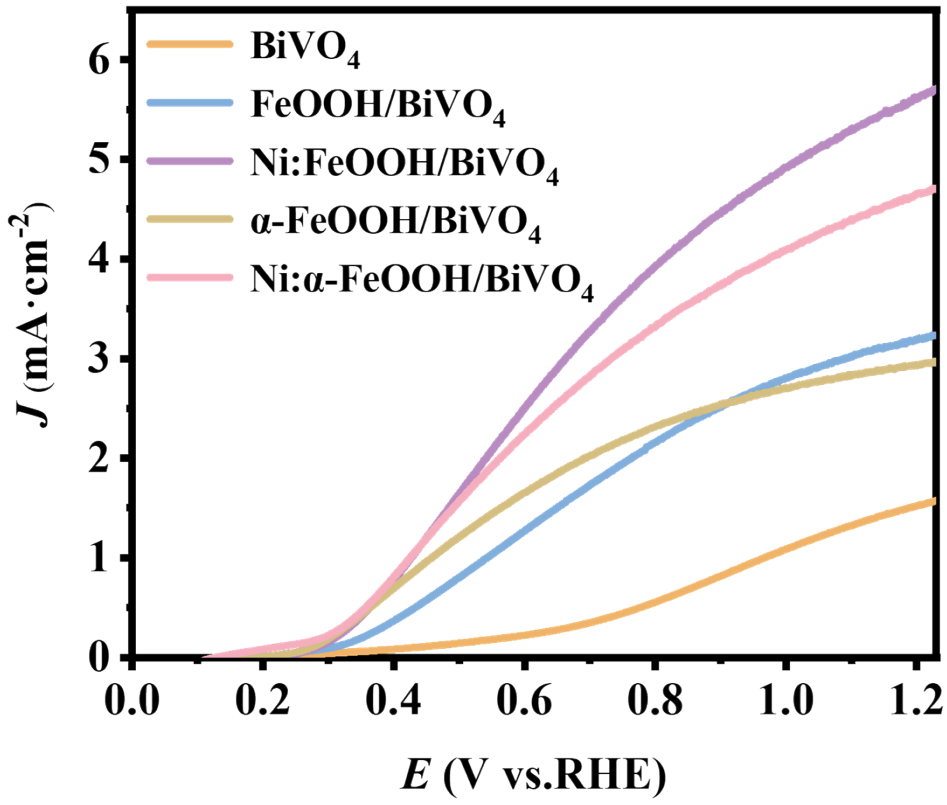

Figure S12. Linear sweep voltammogram curves of $BiVO_4$, α-FeOOH/$BiVO_4$ and Ni:α-FeOOH/$BiVO_4$.

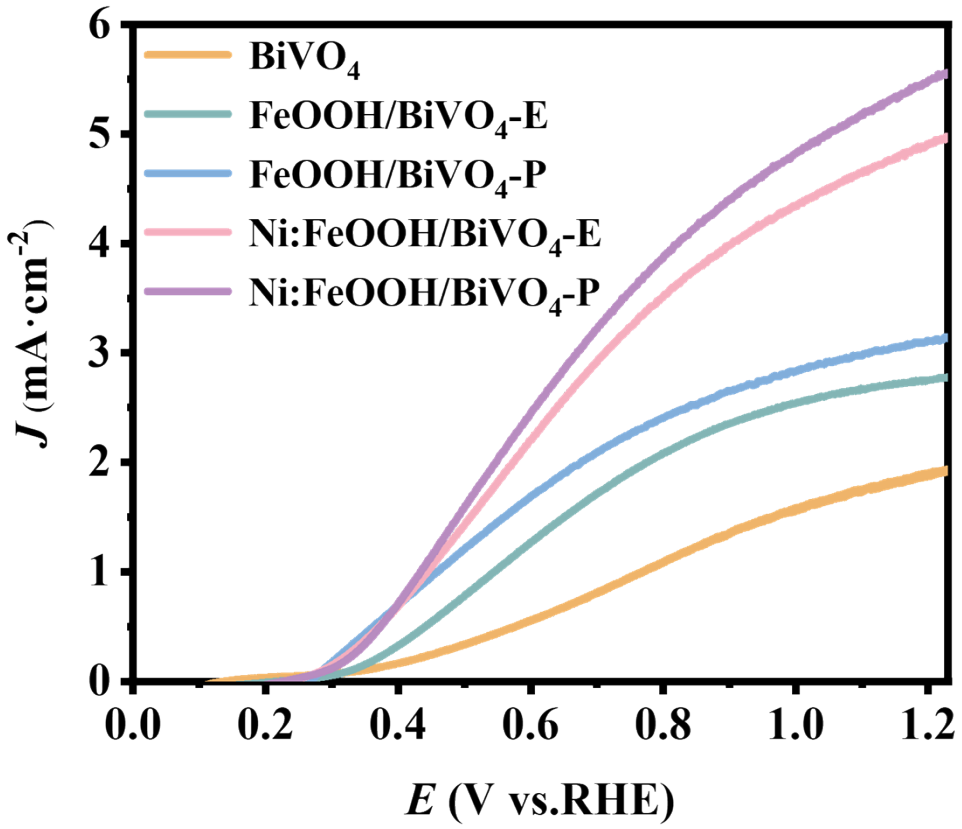

Figure S13. LSV curves of $BiVO_4$, Electrodeposited $FeOOH/BiVO_4$ and Photoelectrochemical deposition of $FeOOH/BiVO_4$.

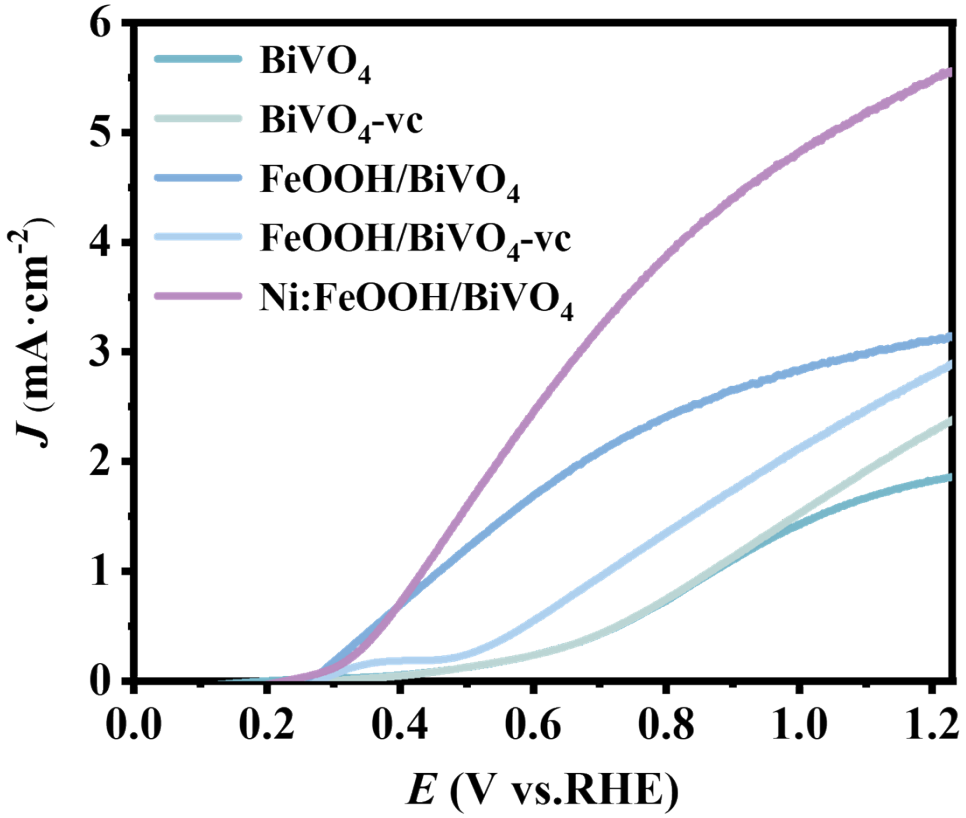

Figure S14. LSV curves of $BiVO_4$, $BiVO_4$-vc, FeOOH/$BiVO_4$ and FeOOH/$BiVO_4$-vc.

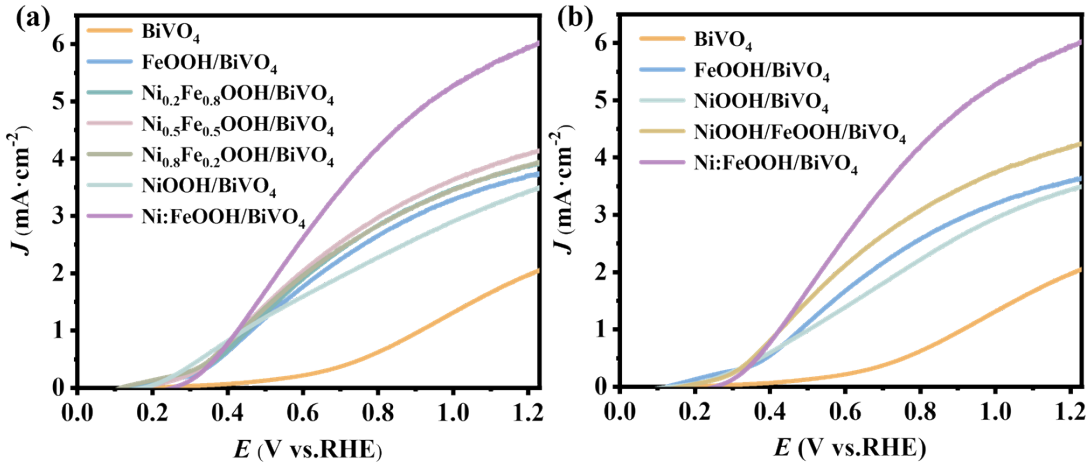

Figure S15. LSV curves of (a) NiFeOOH/$BiVO_4$ with varying NiFe ratios and (b) $BiVO_4$, FeOOH/$BiVO_4$, NiOOH/ $BiVO_4$, NiOOH/FeOOH/$BiVO_4$ and Ni:FeOOH/$BiVO_4$.

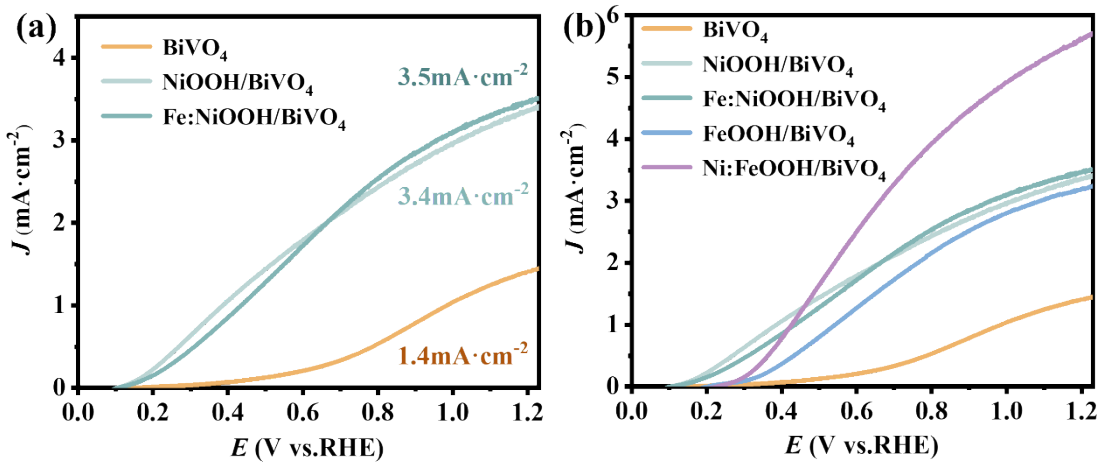

Figure S16. LSV curves of (a) $BiVO_4$, $NiOOH/BiVO_4$, $Fe:NiOOH/BiVO_4$ and (b) he photocathode before and after the replacement of FeOOH and NiOOH.

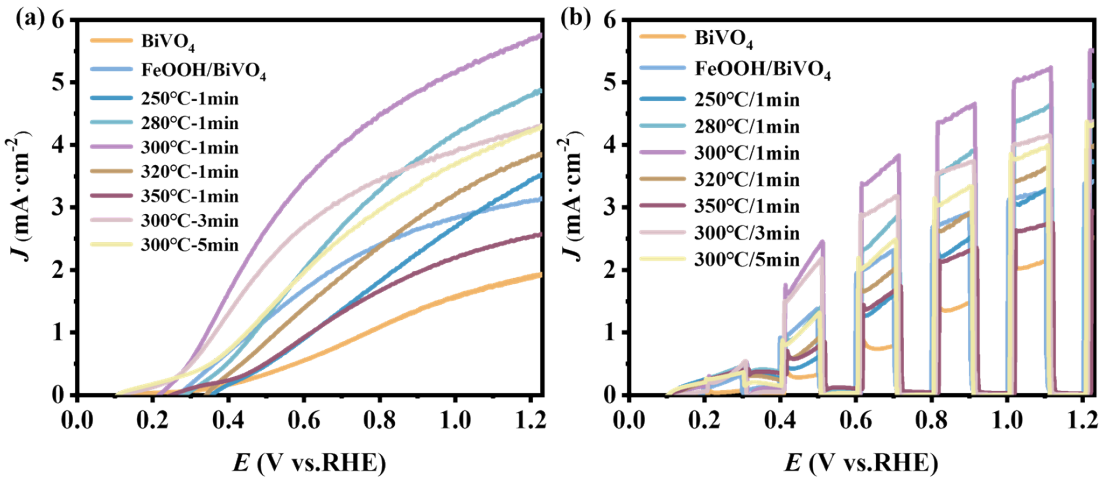

Figure S17. Chopping LSV curves of $BiVO_4$, $FeOOH/BiVO_4$ and $Ni:FeOOH/BiVO_4$ measured in 0.2 M borate buffer (pH = 8.4) electrolyte.

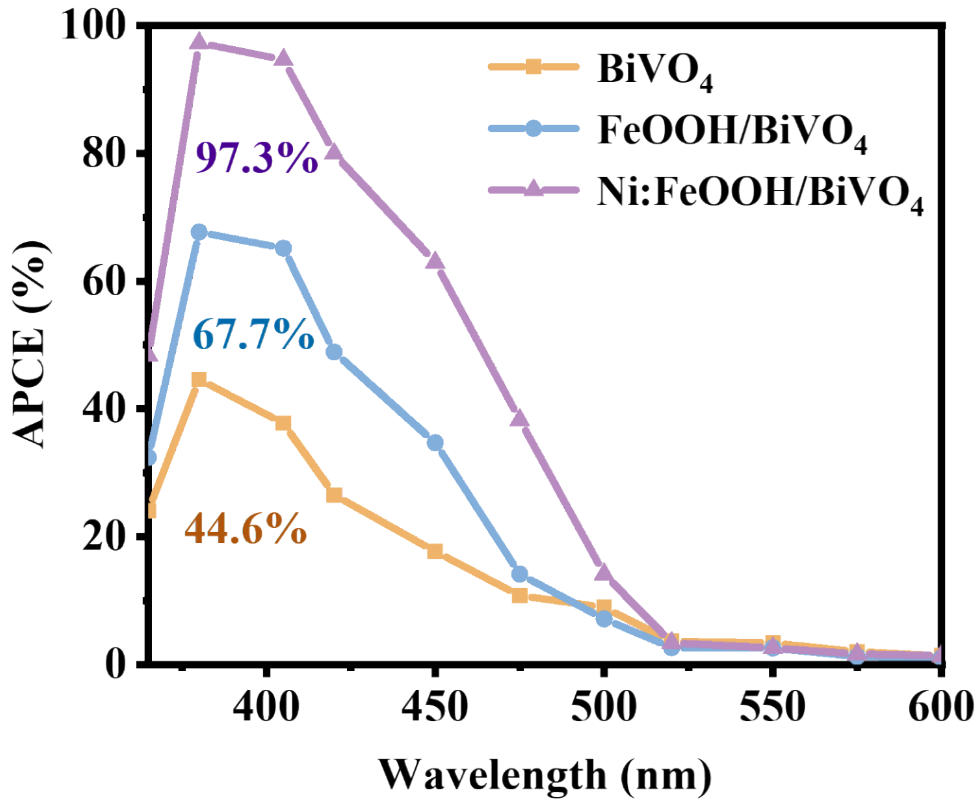

Figure S18. APCE curves of different photoanodes at 1.23 V_{RHE} under AM 1.5G illuminations.

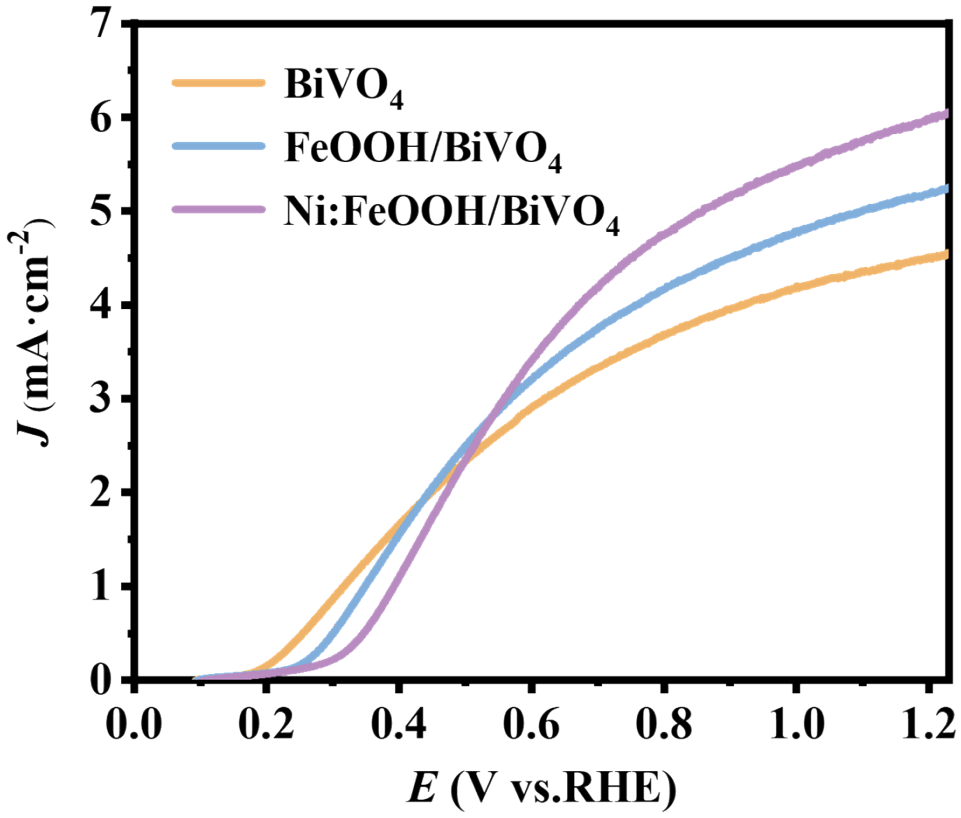

Figure S19. LSV curves of $BiVO_4$, $FeOOH/BiVO_4$ and $Ni:FeOOH/BiVO_4$ measured in 0.2 M borate buffer (pH = 8.4) electrolyte with 0.2 M Na_2SO_3.

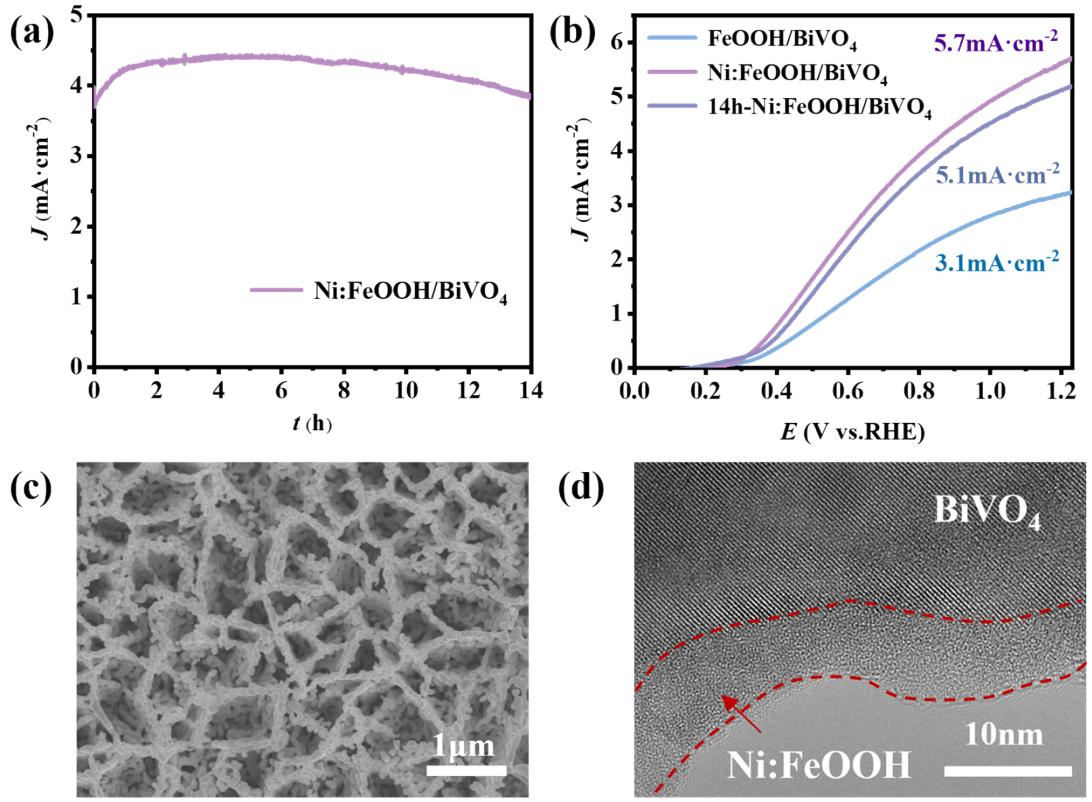

Figure S20. (a) J-T curves of Ni:FeOOH/$BiVO_4$ at 0.8 V_{RHE}, (b) LSV curves, (c) SEM and (d) TEM of Ni:FeOOH/$BiVO_4$ after stability test.

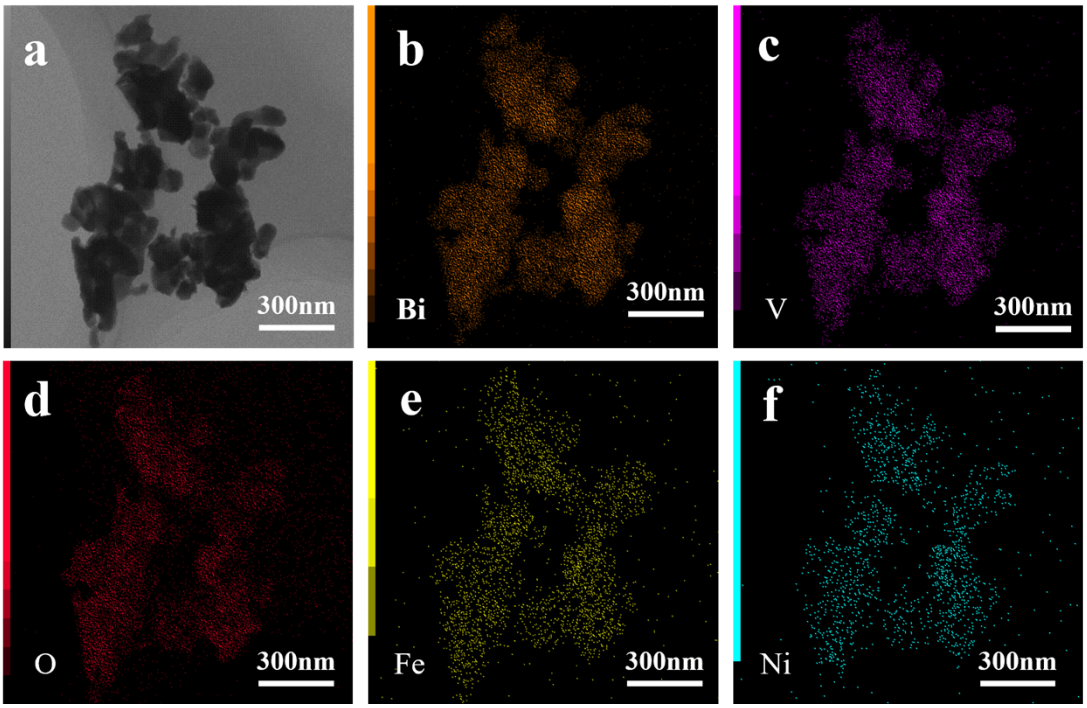

Figure S21. TEM EDS of 14h-Ni:FeOOH/$BiVO_4$.

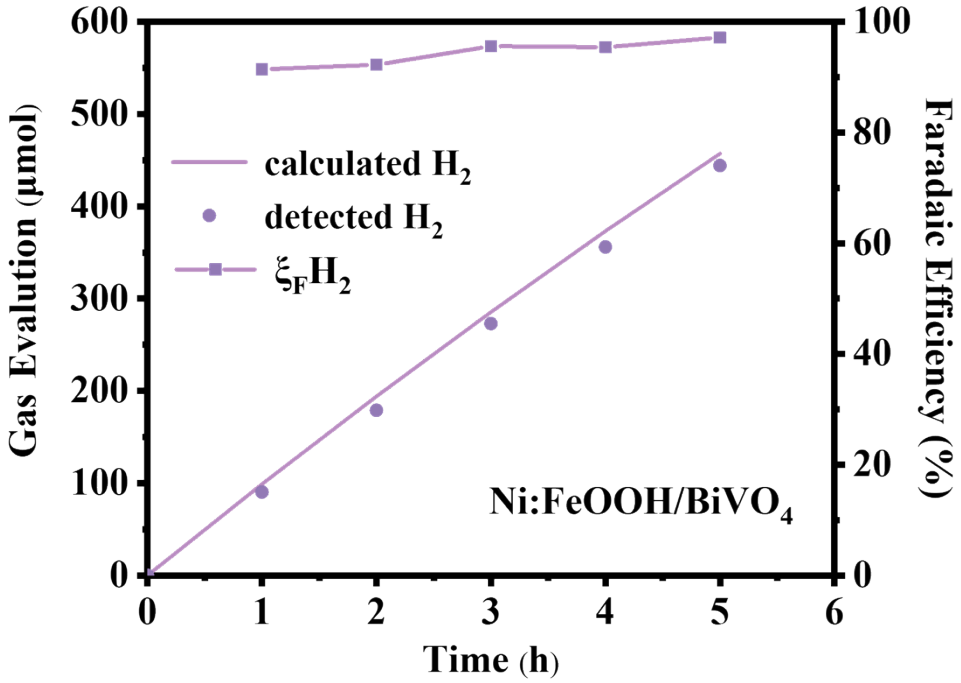

Figure S22. Faradaic efficiency and gas evolution at 1.23 V_{RHE} of Ni:FeOOH/$BiVO_4$ photoanode.

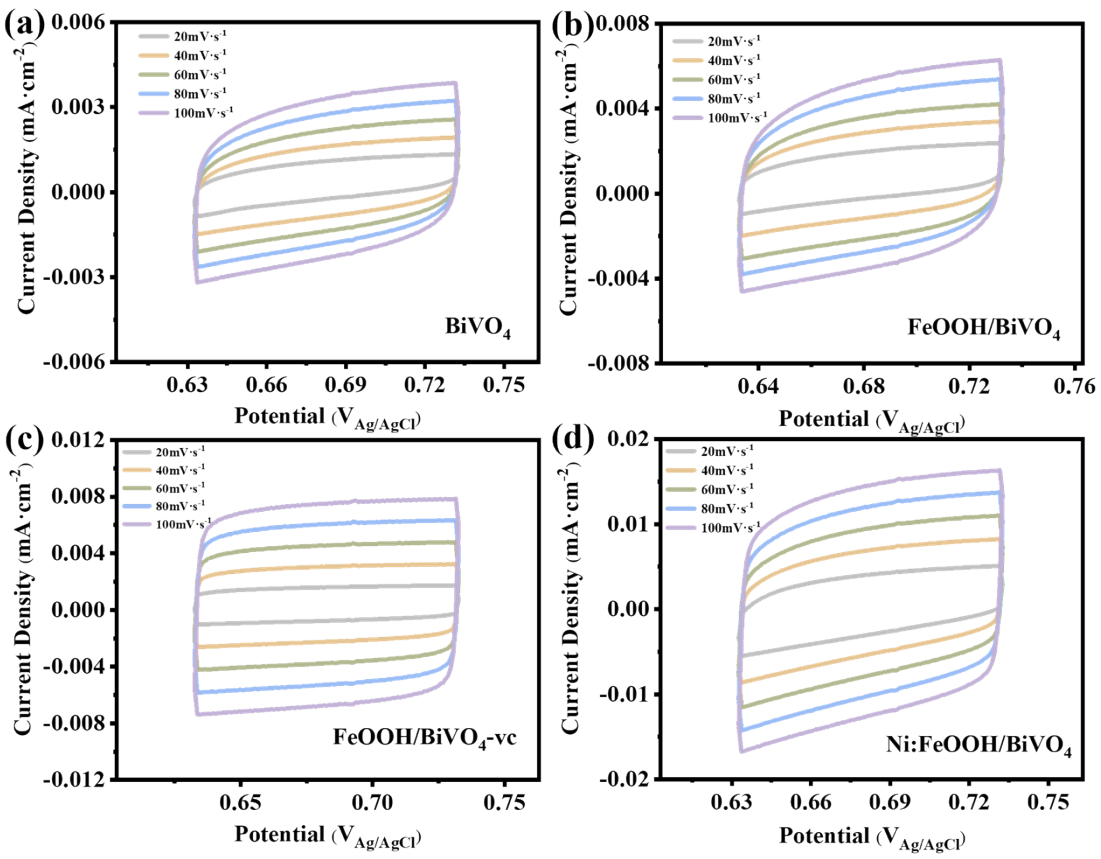

Figure S23. CV curves of (a) $BiVO_4$ (b) $FeOOH/BiVO_4$ (c) $FeOOH/BiVO_4$-vc and (d) $Ni:FeOOH/BiVO_4$.

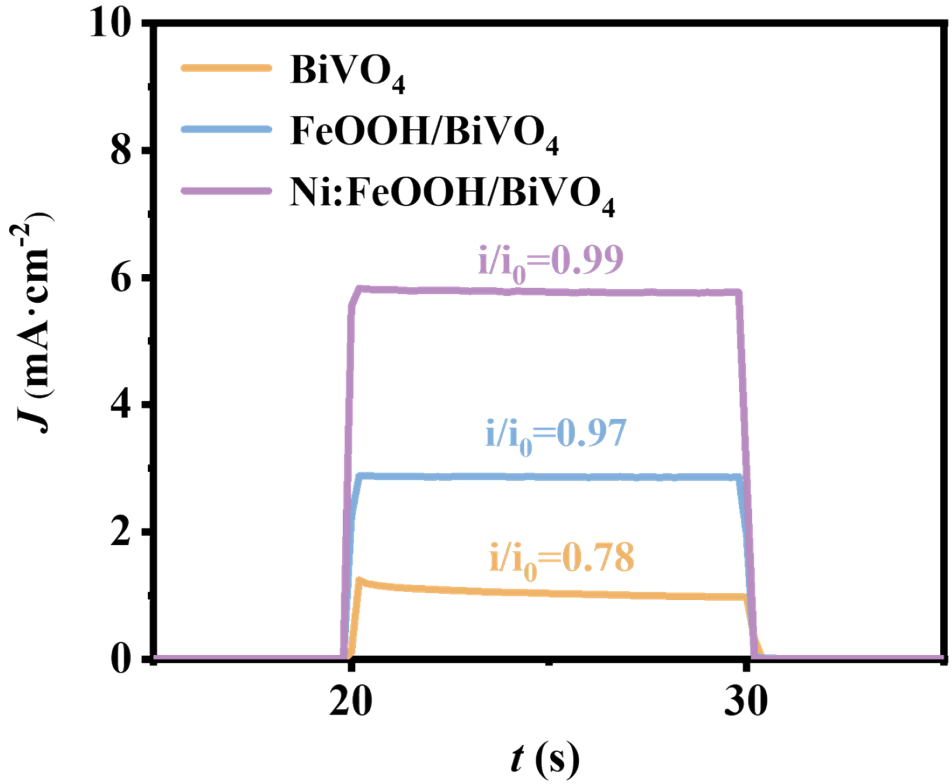

Figure S24. The transient photocurrent decay curves of $BiVO_4$, $FeOOH/BiVO_4$ and $Ni:FeOOH/BiVO_4$.

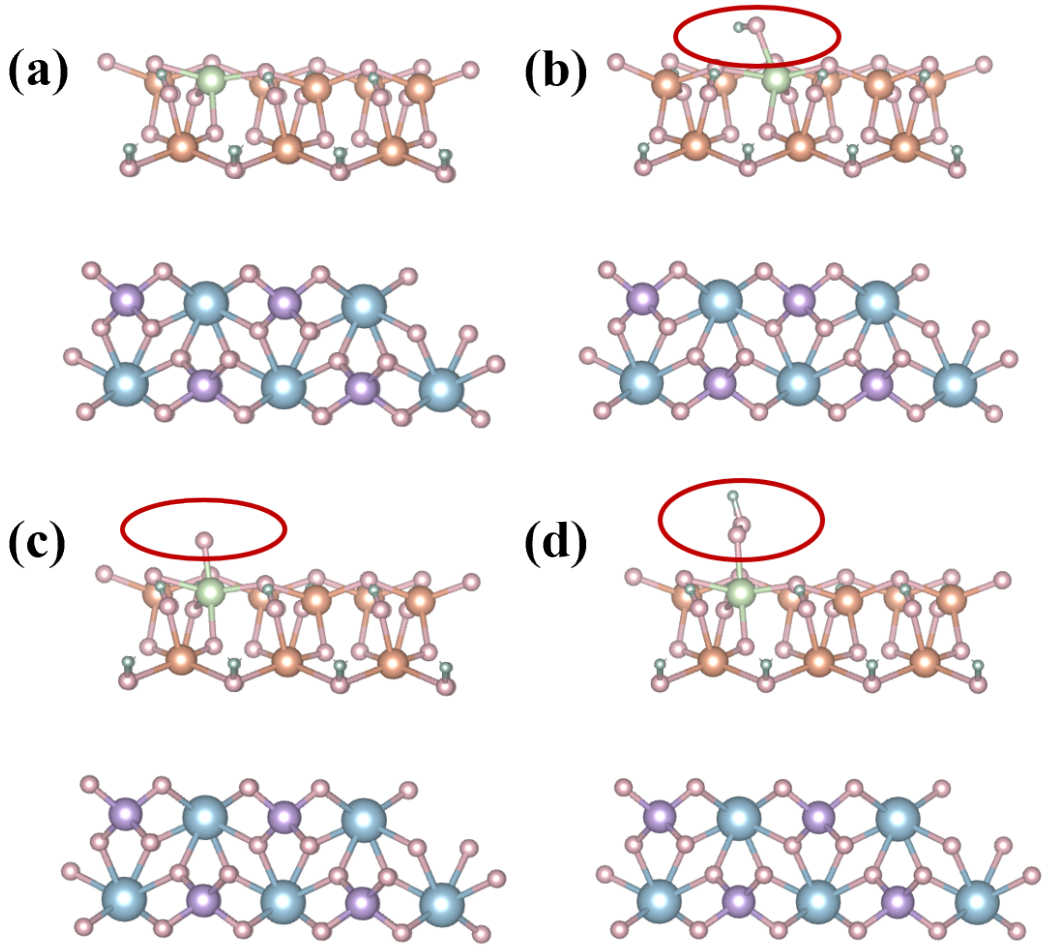

Figure S25. The optimized configurations of *OH, *O, and *OOH adsorbed on Ni:FeOOH/$BiVO_4$ for OER.

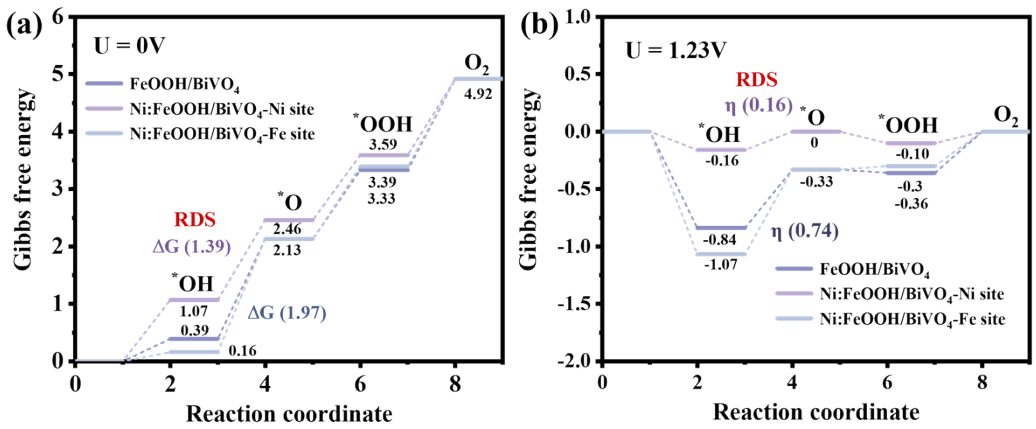

Figure S26. The corresponding Gibbs free energy diagrams of each step of OER at Fe and Ni active sites under conditions of (a) 0 V and (b) 1.23 V.

Table S1. SEM elemental content ratio of Bi, V, O, Fe, Ni of Ni:FeOOH/$BiVO_4$.

Elements	Bi	V	O	Fe	Ni
wt%	65.26	14.69	19.76	0.21	0.08
at%	16.96	15.67	67.09	0.20	0.07

Table S2. ICP of Bi, V, O, Fe, Ni of FeOOH/$BiVO_4$ and Ni:FeOOH/$BiVO_4$.

Elements	Bi	V	Fe	Ni
FeOOH/$BiVO_4$	47.0%	46.2%	6.8%	
Ni:FeOOH/$BiVO_4$	43.5%	43.2%	7.1%	6.2%

Table S3. XPS peak positions of $BiVO_4$, FeOOH/$BiVO_4$ and Ni:FeOOH/$BiVO_4$ O 1s.

Sample	O_L (eV)	O_H (eV)	O_C (eV)
$BiVO_4$	529.71	531.41	532.64
FeOOH/$BiVO_4$	529.80	531.37	532.27
Ni:FeOOH/$BiVO_4$	529.85	531.45	532.43

Table S4. XPS area ratio of $BiVO_4$, $FeOOH/BiVO_4$ and $Ni:FeOOH/BiVO_4$ O 1s.

Sample	O_L	O_H	O_C
$BiVO_4$	78.7%	17.3%	4.0%
$FeOOH/BiVO_4$	38.6%	37.5%	23.9%
$Ni:FeOOH/BiVO_4$	44.2%	43.0%	12.8%

Table S5. SEM elemental content ratio of Bi, V, O, Fe, Ni of $Fe:NiOOH/BiVO_4$.

Elements	Bi	V	O	Fe	Ni
wt%	65.65	14.72	19.35	0.07	0.21
at%	17.28	15.91	66.53	0.07	0.21

Table S6. TEM elemental content ratio of Bi, V, O, Fe, Ni of 14h-$Fe:NiOOH/BiVO_4$.

Sample		Bi	V	O	Fe	Ni
$Ni:FeOOH/BiVO_4$	atoms%	26.99	16.22	55.01	1.57	0.21
14h-$Ni:FeOOH/BiVO_4$	atoms%	25.65	15.57	57.21	1.42	0.15

Table S7. Comparison of our work with recent $BiVO_4$ photoanodes modified with cocatalyst for PEC water oxidation at 1.23 V_{RHE} under AM 1.5G (100 $mW \cdot cm^{-2}$) illumination.

Photoelectrode	J($mA \cdot cm^{-2}$)	ABPE(%)	η_{inj}(%)	η_{sep}(%)	Stability(h)	Ref.
$Ni_3POM/FeOOH/BiVO_4$	5.20	1.10	74.8	69.3	1	[8]
$B\text{-}BiVO_4/Fe_xCo_{1-x}OOH$	5.21	2.05	90.6	69.5	8	[9]
$Ni:FeOOH\text{-}Vo/BiVO_4$	4.15	1..62	61.9	89.7	5	[10]
$CoTAA/FeOOH/BiVO_4$	4.97	1.66	77.1	66.3	3	[11]
$Fe:Ni/BiVO_4$	4.72	1.67	90.9	98.1	8	[12]
$BiVO_4/FeOOH/TANi$	4.60	1.3	88.5	61.3	3	[13]
$Ni/BiVO_4$	4.41	1.92	81.6	95.8	10	[14]
$BiVO_4/F/CoS\text{-}NIR$	4.86	1.56	89.2	87.7	3	[15]
$BiVO_4/PDA/\beta\text{-}FeOOH$	4.84	1.52	79.6	80.9	8	[16]
$BiVO_4/ZnCo\text{-}MOFs/NiFeBi$	4.40	1.30	62.8	93.5	4	[17]
$Ni(OH)_2/Cl\text{-}BiVO_4$	4.33	1.13	76.9	83.7	3	[18]
$NiFe\text{-}MOFs/\ BiVO_4$	4.61	1.81	70	83	3	[19]
$M\text{-}CoS/BiVO_4$	5.22	1.58	83.4	84.2	8	[20]
$BiVO_4/TAFC$	4.97	1.48	78.9	82.0	3	[21]
CuMTZ/BVO	3.32	1.04	89.0	69.0	3	[22]
$NiFe/CA/Fe\text{-}BiVO_4$	6.2	2.15	86.1	96.8	12	[6]
$NiCoFe\text{-}Bi/CuSCN/BiVO_4$	5.6	2.31	84.6	84.5	10	[23]
$O_v\text{-}BiVO_4/MIL\text{-}101$	5.91	2.15	86.0	92.0	3.5	[24]
$Ni:FeOOH/BiVO_4$	5.71	1.74	94.5	80.6	10	This work

Table S8. The values of N_d and the slope of the M-S plots.

Sample	Slope ($\times 10^9$)	Nd ($\times 10^{18}$, cm^{-3})	E_{fb} (V)
$BiVO_4$	5.47	3.79	0.35
$FeOOH/BiVO_4$	3.85	5.39	0.34
$Ni:FeOOH/BiVO_4$	3.36	6.17	0.31

Table S9. The charge transfer resistance (Rct) of electrodes.

Sample	Rs(Ω)	Rct(Ω)	CPE(F)
$BiVO_4$	38.64	253.60	2.67E-5
$FeOOH/BiVO_4$	41.20	15.15	6.71E-5
$Ni:FeOOH/BiVO_4$	38.73	13.83	1.91E-5

Table S10. Free energy changes four elementary steps for OER in $BiVO_4$, $FeOOH/BiVO_4$, $Ni:FeOOH/BiVO_4$-Ni sites and $Ni:FeOOH/BiVO_4$-Fe sites systems at 0 V and 1.23 V, and the free energy unit is eV.

Sample	U(V)	Step 1	Step 2	Step 3	Step 4
$BiVO_4$	0	2.57	2.43	0.10	-0.17
	1.23	1.34	1.20	-1.13	-1.40
$FeOOH/BiVO_4$	0	0.39	1.74	1.20	1.59
	1.23	-0.81	0.51	-0.03	0.36
$Ni:FeOOH/BiVO_4$-Ni sites	0	1.08	1.39	1.13	1.32
	1.23	-0.16	0.16	-0.10	0.10
$Ni:FeOOH/BiVO_4$-Fe sites	0	0.16	1.97	1.26	1.53
	1.23	-1.07	0.74	0.03	0.30

References

1. D. Seo, D. H. Wi and K. S. Choi, Enabling solar water oxidation by $BiVO_4$ in strongly acidic solutions. *Journal of the American Chemical Society*, 2025, **147**, 35002-35010.
2. L. Fu, Z. Li, X. Shang and W. Zhang, M-O-M bond mediated three-dimensional materials accelerates photoelectrochemical kinetics across length scales and timescales. *Applied Catalysis B: Environment and Energy*, 2025, **379**, 125732.
3. J. Yang, C. Deng, Y. Lei, M. Duan, Y. Yang, X. Chen, S. Yang, J. Li, H. Sheng, W. Shi, C. Chen and J. Zhao, Fe-N Co-doped $BiVO_4$ photoanode with record photocurrent for water oxidation. *Angewandte Chemie International Edition*, 2025, **64**, 202416340.
4. L. Geronimo, C. G. Ferreira, V. Gacha, D. Raptis, J. Martorell and C. Ros, Understanding the internal conversion efficiency of $BiVO_4/SnO_2$ photoanodes for solar water splitting: An experimental and computational analysis. *ACS Applied Energy Materials*, 2024, **7**, 1792-1801.
5. Y. Su, Y. Yu, T. Xue, K. Teng, Y. Fan, J. Lin, C. Liu, Q. Qu and L. Li, Revolutionary photoelectrochemical water splitting performance of $BiVO_4/Bi_2S_3$ heterojunction photoanodes boosted by trace bio-Cr_2O_3 through multiple mechanisms. *Chemical Engineering Journal*, 2025, **517**, 164376.
6. X. Li, J. Wu, C. Dong, Y. Kou, C. Hu, J. Zang, J. Zhu, B. Ma, Y. Li and Y. Ding, Boosting photoelectrocatalytic oxygen evolution activity of $BiVO_4$ photoanodes via caffeic acid bridged to NiFeOOH. *Applied Catalysis B: Environment and Energy*, 2024, **353**, 124096.
7. K. Tian, L. Jin, A. Mahmood, H. Yang, P. An, J. Zhang, Y. Ji, Y. Li, D. Li, S. Liu and J. Yan, Lattice Distortion Promotes Carrier Separation to Improve the Photoelectrochemical Water Splitting Performance of Bismuth Vanadate Photoanode. *Advanced Functional Materials*, 2024, **34**, 2410548.
8. C. Hu, C. Xu, X. Li, B. Li, X. Ma, J. Zhu, C. Dong and Y. Ding, Coupling Ni_3POM with FeOOH on $BiVO_4$ photoanodes for efficient photoelectrochemical water splitting. *ACS Sustainable Chemistry & Engineering*, 2023, **11**, 7367-7377.
9. Z. Kang, Z. Sun, Y. Zang, S. Wan, Y.-Z. Zheng and X. Tao, Dual functions of heterometallic FeCo oxyhydroxides in borate-treated $BiVO_4$ photoanodes toward boosted activity and photostability in photoelectrochemical water oxidation.

Chemical Engineering Journal, 2022, **431**, 133379.

10. M. A. Gaikwad, U. V. Ghorpade, U. P. Suryawanshi, P. V. Kumar, S. Jang, J. S. Jang, L. Tran, J. S. Lee, H. Bae, S. W. Shin, M. P. Suryawanshi and J. H. Kim, Rapid synthesis of ultrathin Ni:FeOOH with in situ-induced oxygen vacancies for enhanced water oxidation activity and stability of $BiVO_4$ photoanodes. *ACS Applied Materials & Interfaces*, 2023, **15**, 21123-21133.
11. L. Zhu, Z. Liang, S. Zhu, Y. Cheng, Z. Li, H. Du, C. Zhu, D. Jiang and Y. Yuan, Regulating the binding strength of oxygen intermediates with a conductive π–d conjugated metal-organic polymer CoTAA on $BiVO_4$ photoanode for efficient photoelectrochemical water oxidation. *Chemical Engineering Journal*, 2024, **483**, 149400.
12. X. Cao, Q. Dang, H. Chen, Y. Zhao, Y. Liu, J. Zeng, Q. Ma, L. Zhong, D. Wang and Y. Qiu, Fe-doped Ni nanocrystals as a cocatalyst for efficient $BiVO_4$ photoanode: Mechanism insights into Fe-accelerated in-situ reconstruction. *Applied Surface Science*, 2025, **711**, 164083.
13. T. Tian, G. Jiang, Y. Li, W. Xiang and W. Fu, Unveiling the activity and stability of $BiVO_4$ photoanodes with cocatalyst for water oxidation. *Renewable Energy*, 2022, **199**, 132-139.
14. P. Wen, R. Lei, X. Cao, Q. Ma, G. Zhang, C. Guo, X. Wang and Y. Qiu, Anchored Ni nanocrystals boosting $BiVO_4$ photoanode for highly efficient water oxidation via in-situ generation of Ni@NiOOH co-catalyst. *Chemical Engineering Journal*, 2023, **454**, 139983.
15. H. Li, M. Lyu, Y. Lai, X. Cheng and Z. Dong, Photothermal effect and surface fluorination enable ultrafast charge transfer for efficient photoelectrochemical water oxidation. *Chemical Engineering Journal*, 2025, **515**, 163648.
16. N. Chen, L. Yu, C. Liu, Z. Li, Y. Zhang and H. Zhu, Polydopamine-mediated hydrogen bond network promotes hole extraction in $BiVO_4$ photoanodes for efficient photoelectrochemical water oxidation. *Journal of Materials Chemistry A*, 2025, **13**, 17528-17540.
17. W. Fang, Z. Zhang, Y. Fang, Y. Kan, T. Li, C. Chen, R. Wang, L. Wang and Y. Jia, Synergistic regulation of efficient $BiVO_4$ photoanode by MOF interface band engineering and NiFeBi bimetallic dynamic cocatalyst. *Journal of Environmental Chemical Engineering*, 2025, **13**, 118895.
18. J. Zhang, X. Wei, J. Zhao, Y. Zhang, L. Wang, J. Huang, H. She and Q. Wang,

Electronegative Cl^- modified $BiVO_4$ photoanode synergized with nickel hydroxide cocatalyst for high-performance photoelectrochemical water splitting. *Chemical Engineering Journal*, 2023, **454**, 140081.

19. Y. Li, Q. Wang, X. Hu, Y. Meng, H. She, L. Wang, J. Huang and G. Zhu, Constructing NiFe-metal-organic frameworks from NiFe-layered double hydroxide as a highly efficient cocatalyst for BiVO4 photoanode PEC water splitting. *Chemical Engineering Journal*, 2022, **433**, 133592.
20. D. Li, X. Chen, M. Shao, S. Hou, J. Guo, H. Jin, H. Yang, G. Chen and Y. Huang, Metal–organic framework-derived nano-CoS-enhanced photoelectrochemical water splitting performance of the $BiVO_4$ photoanode. *Journal of Materials Chemistry A*, 2025, **13**, 22652-22659.
21. H. Huang, Z. Zhang, W. Xie, B. Fan, C. Wu, R. Jiang, J. Huang, B. Zhang, Y. Hou and Z. Yu, Ultrathin layer TAFC on $BiVO_4$ with ligand-to-metal charge transfer enhances built-in electric field for boosting photoelectrochemical water oxidation. *Journal of Colloid and Interface Science*, 2024, **668**, 551-564.
22. J.-W. Ji, L.-J. Zhang, H.-C. Wang, Y.-X. Duan, X.-Z. Yue, J.-H. Chen and S.-S. Yi, Ligand doping engineering induced robust internal electric field in MOFs/$BiVO_4$ photoanode for water splitting. *Chemical Engineering Journal*, 2024, **484**, 149597.
23. Y. Liu, Z. Zhang, K. Wang, X. Tan, J. Chen, X. Ren and F. Jiang, Efficient $BiVO_4$ photoanode with an excellent hole transport layer of CuSCN for solar water oxidation. *Advanced Energy Materials*, 2024, **14**, 2304223
24. Y. Xin, J. Tian, X. Xiong, C. Wu, S. A. C. Carabineiro, X. Yang, Z. Chen, Y. Xia and Y. Jin, Enhanced photocatalytic efficiency through oxygen vacancy-driven molecular epitaxial growth of metal-organic frameworks on $BiVO_4$. *Advanced Materials*, 2025, **37**, 2417589.